

Received XX Month, XXXX; revised XX Month, XXXX; accepted XX Month, XXXX; Date of publication XX Month, XXXX; date of current version XX Month, XXXX.

Digital Object Identifier 10.1109/OJCAS.2025.1234567

Nonlinear Analysis of Differential LC Oscillators and Injection Locked Frequency Dividers

Konstantinos Metaxas¹, Vassilis Alimisis^{1,3} (Member, IEEE), Costas Oustoglou¹, Yannis Kominis² and Paul P. Sotiriadis^{1,3} (Fellow, IEEE)

¹School of Electrical and Computer Engineering, National Technical University of Athens, 15780 Athens, Greece

²School of Applied Mathematical and Physical Sciences, National Technical University of Athens, 15780 Athens, Greece

³Archimedes/Athena RC, 15125 Marousi, Greece

Corresponding author: Konstantinos Metaxas (email: kostismetaxas@yahoo.com).

The publication of the article in OA mode was financially supported in part by HEAL-Link.

ABSTRACT A comprehensive nonlinear analysis of autonomous and periodically forced fully-differential, negative-resistor LC oscillators is presented. Through nonlinear transformations in the state space, it is shown that oscillators within this class exhibit qualitatively similar dynamical behavior in terms of their limit cycles and bifurcation curves, at least within an open region containing the origin. The case of autonomous, complementary BJT oscillators is used to validate the qualitative analysis and demonstrate a general approach of how to numerically extend the bifurcation curves away from the equilibrium point and determine the oscillatory conditions. When external periodic force is present, we focus on the special case of periodically multiplicatively-forced fully-differential, negative-resistor, LC oscillators and use Harmonic Balance techniques to derive analytical expressions estimating the locking range in the weak injection regime. The results are used to calculate the locking range of a harmonically forced complementary BJT oscillator yielding explicit expressions closely aligned with experimental measurements, thus verifying the validity of the analysis.

INDEX TERMS Bifurcation analysis, injection-locked frequency dividers (ILFDs), locking range (LR), nonlinear oscillators, harmonic balance, synchronization, frequency dividers.

I. Introduction

Frequency dividers are widely used in communication applications and constitute an important building block of phase-locked loops (PLLs) [1]. Their primary function is to divide an input frequency by an integer, which serves as the input to further layers operating at lower frequencies [1], [2]. While digital implementations are possible, analog injection-locked frequency dividers (ILFDs) offer an alternative due to their lower power consumption [1], [2]. In particular, differential LC dividers constitute a very common architecture [3].

ILFDs can be mathematically viewed as periodically forced limit cycle oscillators. The analysis of the autonomous systems, i.e. without external excitation, in terms of their design parameters is crucial for identifying the regions on the parameter space where oscillations occur. The study of the qualitative changes in the behavior – e.g. creation and

destruction of fixed points, limit cycles, strange attractors or stability changes – of a dynamical system, as its intrinsic parameters are varied, is known as *bifurcation analysis* in the applied mathematics literature [4]–[6]. This concept is closely related to identifying similarities in the behavior of different systems within certain parameter regions, formally known as *topological equivalence*, and has been central to the study of dynamical systems since the time of Poincaré [6]. Various bifurcation analyses have been successfully applied to ecological [7], mechanical [8], optical [9], [10] and electronic [1], [11], [12] systems, as well as to fusion plasmas [13] and neuroscience [14], in order to analyze the dynamical complexity. Regarding autonomous differential LC oscillators, although bifurcation analysis has been conducted for the specific MOS architecture [1], which involves a particular type of cubic nonlinearity, it has not been demonstrated that

the mechanism governing the creation and destruction of oscillations is qualitatively consistent across all nonlinear circuits in this class. This in turn, gives a theoretical and a quantitative –when the bifurcation curves are numerically computed for the exact system– guide for appropriately selecting the parameters of the systems that will be utilized as a divider.

Due to the nonlinear nature of synchronization [15], [16], the range of input frequencies for which phase locking occurs in a periodically forced limit cycle oscillator is restricted, typically referred to as the *locking range* (LR). Various methods have been proposed to estimate the LR under weak injection conditions. These include Adler's equations [17], averaging methods [18]–[27], qualitative analyses [1], first-order approximations of phase reduction models [2], [28]–[31], perturbation methods [32] and harmonic balance methods [33]–[45]. The latter class of methods generalizes the results of Adler [17], enabling analytical estimation of the locking range in a straightforward manner.

In this work, we begin with the study of autonomous differential LC oscillators and demonstrate that, through appropriate nonlinear transformations, their dynamical behavior is qualitatively the same, at least in a neighborhood of the origin. Utilizing the complementary BJT oscillator as an example, we numerically determine the bifurcation curves, verifying and extending the qualitative analysis away from the origin. The computation of the curves also provides insight into the appropriate selection of parameters for the system when used as a divider. Subsequently, we present a general methodology to estimate the locking range when differential LC oscillators are forced by an arbitrary periodic perturbation, utilizing the harmonic balance technique. This approach, unlike other possible methodologies, enables the deduction of quantitative, analytical results that can be used as a first order estimation during the design of a divider. The application of this method to estimate the locking range (LR) of the complementary BJT ILFD, depicted in Fig. 2, demonstrates close correspondence with the experimental measurements of the implemented circuit in Fig. 7. Our analysis complements and generalizes the results presented in [46] for the particular case of the BJT oscillator.

The paper is organized as follows. In Section II, we show that all differential LC oscillators demonstrate the same qualitative dynamical phenomena and determine numerically the bifurcation curves for the complementary BJT oscillator. In Section III, we analyze the periodically forced differential LC oscillators and derive analytical expressions for the locking range. In Section IV, we conclude the paper.

II. Bifurcation Analysis of Differential LC Oscillators

Consider the equivalent model of the differential LC oscillator in Fig. 1. It is comprised of the LC resonator (tank) and the negative resistance modeled by the voltage-controlled current source $i_c = I_0 f(v/V_r)$, where V_r is a voltage normalization parameter and I_0 has current dimensions.

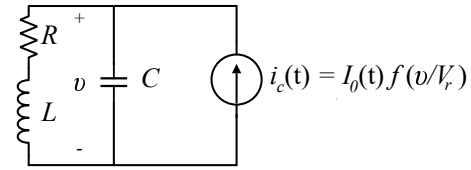


FIGURE 1. Equivalent model of a general class of nonlinear LC oscillators - also operating as frequency dividers when properly injected with periodic signal via $I_0(t)$.

Note that i_c is proportional to I_0 , which is constant if the oscillator is autonomous and time-dependent ($I_0 = I_0(t)$) if the oscillator is externally forced. Thus, in the present Section, where we analyze the dynamical behavior of the free-running model of Fig. 1, I_0 is constant, while in Section III, the injection of an external periodic signal will be modeled as an explicit dependence of I_0 on the time t .

Function $f : \mathbb{R} \rightarrow \mathbb{R}$ is assumed to be odd and at least three times continuously differentiable, i.e., $f \in C^3(\mathbb{R}, \mathbb{R})$, with $f'(0) > 0$ and $f^{(3)}(0) < 0$ (i.e. compressive). Without loss of generality we further assume that $f'(0) = 1$ implying that $f(x) = x - cx^3 + O(x^5)$ with constant $c > 0$.

Let i be the inductor's current. The dynamical system describing the model is

$$\begin{aligned} C \frac{dv}{dt} &= -i + I_0 f(v/V_r) \\ L \frac{di}{dt} &= v - Ri. \end{aligned} \quad (1)$$

Setting $\omega_0 = 1/\sqrt{LC}$ and introducing the change of variables

$$x = \frac{v}{V_r}, \quad y = \frac{Ri}{V_r} \quad \text{and} \quad \tau = \omega_0 t, \quad (2)$$

system (1) is transformed to the dimensionless equivalent one,

$$\begin{aligned} \dot{x} &= -Qy + QGf(x) \\ \dot{y} &= \frac{1}{Q}(x - y), \end{aligned} \quad (3)$$

where

$$Q = \frac{1}{R} \sqrt{\frac{L}{C}}, \quad G = \frac{RI_0}{V_r}. \quad (4)$$

System (3) possesses the symmetry $x \rightarrow -x, y \rightarrow -y$, since f is odd. As a result, taking into account that $f(0) = 0$, we conclude that $(0, 0)$ is a trivial equilibrium of the system. These properties motivate us to consider transforming it into a standard form to study the local and global bifurcations. To this end, the change of variables is introduced

$$\begin{aligned} x_1 &= 3Q\sqrt{Gc}x \\ x_2 &= 9Q^2\sqrt{Gc}(-Qy + QGf(x)) \\ \tilde{\tau} &= \frac{\tau}{3Q}, \end{aligned} \quad (5)$$

transforming system (3) into

$$\begin{aligned} \dot{x}_1 &= x_2 \\ \dot{x}_2 &= \mu_1 x_1 + \mu_2 x_2 - x_1^2 x_2 - x_1^3 + O(x_1^5), \end{aligned} \quad (6)$$

where the normal-form parameters μ_1 and μ_2 are defined as

$$\mu_1 = 9Q^2(G - 1), \quad \mu_2 = 3(Q^2G - 1). \quad (7)$$

Truncating the $O(x_1^5)$ terms in (6), results in the parity symmetric Bogdanov-Takens normal form, which is invariant under the transformation $(x, y) \rightarrow (-x, -y)$ (\mathbb{Z}_2 symmetry) [5], [6], whose dynamics is known in the literature and is studied in the following. At the same time, we transform the results concerning the bifurcation curves of the normal-form parameters (μ_1, μ_2) back to the more important design parameters (G, Q) , ensuring consistency with the numerical analysis for the specific nonlinearity f arising from the architecture discussed in the next subsection. Henceforth, when referring to (6) we will mean the truncated system. A typical (generic) bifurcation diagram of (6) with respect to the μ_1, μ_2 parameters is shown in Fig. 3 (a).

For $\mu_1, \mu_2 < 0$ the origin is the unique equilibrium of the system, which is stable. At $\mu_2 = 0, \mu_1 < 0$ (corresponding to $G < 1, Q^2G = 1$), the origin becomes unstable and a stable limit cycle, corresponding to a small-amplitude oscillation, emerges. Thus, a supercritical Hopf bifurcation [4]–[6], denoted by $H^{(1)}$ in the parameter plane, occurs. For $\mu_1 < 0, \mu_2 > 0$ the limit cycle is the unique attractor and the origin the unique repeller of the system [4]–[6]. At $\mu_1 = 0$ (corresponding to $G = 1$), the origin becomes a saddle and a pair of symmetric, with respect to the origin, unstable equilibria is created [4], [6]. This suggests that a pitchfork bifurcation [4]–[6], denoted by $F_+^{(1)}$ in the parameter plane, has occurred. The symmetric equilibria are unstable for parameter values $\mu_2 > \mu_1 > 0$. At $\mu_1 = \mu_2$ (corresponding to $2G - 3 = -1/Q^2$) they become stable, while simultaneously, two symmetric, with respect to the origin, unstable cycles are created around them [4], [6]. This scenario is the inverse of the supercritical Hopf bifurcation discussed at $\mu_2 = 0$ and $\mu_1 = 0$, and corresponds to a subcritical Hopf bifurcation, denoted as $H^{(2)}$ in the parameter plane. The two unstable cycles form a homoclinic loop, i.e. a closed orbit of infinite period, at parameter values $\mu_2 = 0.8\mu_1 + O(\mu_1^{3/2})$ (corresponding to $12 - 7G = 5/Q^2$) [4]–[6], [47]. The locus of all such (μ_1, μ_2) is denoted by P in the parameter plane and corresponds to a homoclinic bifurcation. As a result, for parameter values $\mu_1 > \mu_2 > p\mu_1 + O(\mu_1^{3/2}) > 0, p \approx 0.752$, the stable limit cycle and the symmetric stable equilibria are the attractors of the system, while the unstable limit cycle is the unique repeller [4]–[6], [47]. The oscillatory behavior is destroyed at $\mu_2 = p\mu_1 + O(\mu_1^{3/2}), p \approx 0.752$, (corresponding to $G(1 - 3p) + 3p = 1/Q^2$) when the two cycles (stable and unstable) collide and disappear. This scenario corresponds to a typical saddle-node bifurcation, denoted by K in the parameter plane [4]–[6], [47]. As system (6) is a versal deformation [4]–[6], higher-order terms of f do not qualitatively change the dynamics in an open region of the origin. This suggests that, there exists a disk centered at $(x_1, x_2) = (0, 0)$, at least within which all systems resulting from an LC resonator and a differential element, including the MOS implementation of Fig. 2 as described in [1], which is characterized by a cubic nonlinear function f , exhibit the behavior discussed previously for normal-form parameters

(μ_1, μ_2) close to $(0, 0)$, or equivalently, for (G, Q) parameters close to $(1, 1)$. The contribution of higher-order terms shapes the bifurcation curves, particularly in regions distant from the point $(\mu_1, \mu_2) = (0, 0)$, and numerical analysis, as described in the following subsection that considers the exact form of the nonlinearity f , is needed to continue the curves and identify other possible bifurcations.

Concluding the discussion on the normal form (8), we note that the parameters (μ_1, μ_2) determine the dynamical characteristics of the autonomous system (8). Although in the parameter region defined by $H^{(1)}$ and K (cf. Fig. 3), the circuit can operate as an oscillator, the characteristics of the oscillations are not identical, as the autonomous frequency and the rate of convergence—quantified by the Floquet exponents—depend on the parameters (μ_1, μ_2) (cf. the relevant discussion in the next subsection). Additionally, as the parameters vary between the curves $H^{(1)}$ and K , the basin of attraction of the stable limit cycle—namely, the set of initial conditions $(x_1(0), x_2(0))$ for which self-sustained oscillations occur—changes. Specifically, when (μ_1, μ_2) lie between the curves $H^{(1)}$ and K , the initial conditions must lie outside the unstable cycle(s) for oscillatory behavior to manifest. Similar considerations apply to the equilibria and their corresponding convergence speed as well.

Application to the Complementary BJT Oscillator

Consider the oscillator in Fig. 2 (with $v_i = 0$) consisting of two complementary BJT cross-coupled pairs [46]. It is modeled abstractly as in Fig. 1 and therefore its dynamics is captured by system (3) with,

$$f(v/V_r) = \tanh\left(\frac{v}{2V_t}\right), I_0 = \gamma I_{C_{Qn4}}, V_r = 2V_T, \quad (8)$$

where $\gamma = g(\alpha_F)$, $\alpha_F = \beta_F/(\beta_F + 1)$ is the common-base forward short-circuit current gain and $\gamma \rightarrow 1$ as $\alpha_F \rightarrow 1$. The current I_0 , as expected for an autonomous oscillator, is independent of the time t and in fact coincides in this case (ignoring the losses due to $\alpha_F < 1$) with the collector's current.

Fig. 3 (b) shows the bifurcation diagram of system (3) in terms of the design parameters (G, Q) . The super/sub-critical Hopf ($H^{(1,2)}$) bifurcation curves and the pitchfork (P) can be analytically computed as,

$$\begin{aligned} H^{(1)} : Q^2G = 1, P : G = 1, \\ H^{(2)} : (G, Q^2) = \left(\frac{r}{\tanh r}, \frac{\tanh r}{r(1 - \tanh^2 r)} \right), r > 0 \end{aligned} \quad (9)$$

As explained in the previous subsection, the qualitative analysis guarantees the existence of the bifurcation curves and establishes their linear behavior in a neighborhood of the point $(Q, G) = (1, 1)$. Away from this point, the bifurcations cease to be linear and need to be computed numerically, e.g. via [48]. As shown in 3 (b), the continued curves of the nonlinear system (3) locally match the linear ones of the normal form (6) near the point $(\mu_1, \mu_2) = (0, 0)$ and, as expected,

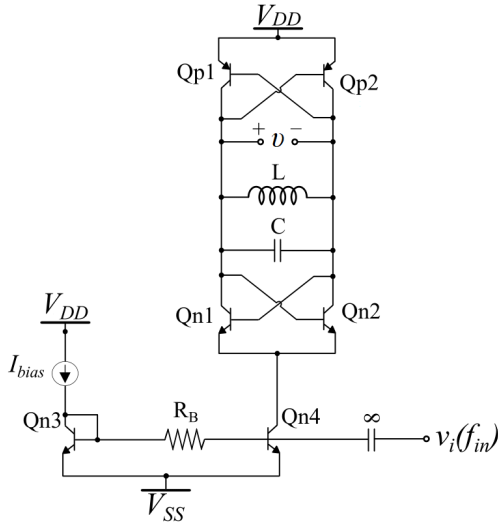


FIGURE 2. LC oscillator consisting of two complementary BJT cross-coupled transistors.

coincide locally with the curves presented in [1] for the MOS implementation characterized by a cubic nonlinear function f . However, the numerical computation of these curves also extends the qualitative behavior analyzed in the previous subsection to the entire parameter space. Thus, the creation and destruction of oscillations are quantitatively determined. We could argue that the qualitative local behavior extends to the whole parameter space whenever the nonlinearity f has exactly three fixed points, including, as special cases, the MOS implementation in [1] and the BJT shown in Fig. 2.

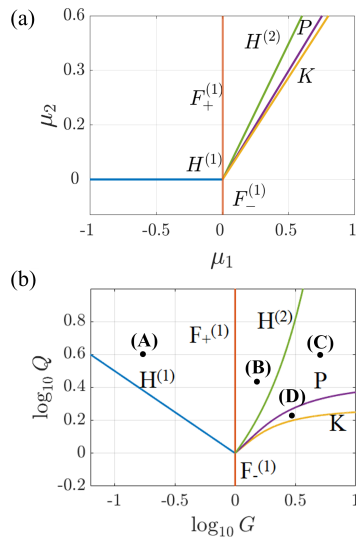


FIGURE 3. (a) Bifurcation diagram with respect to normal-form parameters μ_1, μ_2 around the point $(\mu_1, \mu_2) = (0, 0)$. (b) Bifurcation diagram with respect to design parameters Q, G for the circuit in Fig. 2. The blue line corresponds to a supercritical Hopf bifurcation ($H^{(1)}$), the vertical red line to a pitchfork ($F^{(1)}$), the green to a subcritical Hopf ($H^{(2)}$), the magenta to a homoclinic bifurcation (P) and the orange to a saddle-node (K). Points (A), (B), (C), and (D) correspond to each of the four phase plots shown in Fig. 4.

Qualitatively different phase plots of the system (3) are shown in Fig. 4, for parameter values (G, Q) resulting in a stable limit cycle. Each of the four subfigures in Fig. 4 corresponds to a pair (G, Q) lying in one of the four regions (containing the points A, B, C, and D, respectively) defined by the curves $H^{(1)}, F_+^{(1)}, H^{(2)}, P$, and K in Fig. 3(b), where the system (3) admits self-sustained oscillations.

In (a), the phase space consists of a stable limit cycle and a repeller, the origin, as the parameters lie between the curves $H^{(1)}$ and $F_+^{(1)}$ of Fig. 3 (b). Inside the region defined by the curves $F_+^{(1)}$ and $H^{(2)}$ two unstable equilibria have emerged due to a Pitchfork bifurcation, as depicted in (b). These fixed points gain stability giving rise to two unstable cycles in the region defined by the curves $H^{(2)}$ and P –(c)–, which in turn collide forming a bigger unstable cycle in the region between P and K , as shown in (d). The two cycles –stable and unstable one– finally collide at K . Notably, the qualitative local analysis discussed about the normal is extended on the whole parameter space, as the previous analysis suggests. We remark, as in the analysis of the normal form (6), that although the system (3) admits self-sustained oscillations in each of the four cases, the basin of attraction of the stable limit cycle—namely, the set of initial conditions $(x_1(0), x_2(0))$, or equivalently, the set of initial capacitor voltage and inductor current pairs, for which oscillations are observed—coincides with the entire phase space, except for the origin, i.e., with $(x_1, x_2) \neq (0, 0)$, only in the first case. Therefore, this parameter region is suitable for operation as a divider with weak injection, as it is unlikely for the state-space vector (x, y) to converge to any equilibrium (formally, the measure of the complement of the basin of attraction is zero).

The effects of parameters G and Q on the Floquet multiplier μ and on the oscillation frequency ω of the principal limit cycle, i.e., the stable cycle of Fig. 4, are illustrated in Fig. 5. The curves emerge at different values of the parameter G , corresponding to points (G, Q) lying on the Hopf curve $H^{(1)}$ of Fig. 3. At the birth of the limit cycle, the Floquet multiplier μ always equals 1. Based on the qualitative analysis of the normal form (6) and the discussion on Figs. 3 and 4, the principal oscillation is destroyed when the point (G, Q) lies on the K curve of Fig. 3, where a saddle-node bifurcation occurs. From the perspective of the Floquet multiplier, at this point μ assumes the value 1, as demonstrated for the $\log_{10} Q = 0.1$ case. The same pattern holds for the remaining three curves, although the bifurcation occurs at significantly higher values of the parameter G .

For a fixed $G < 1$, i.e., between the $H^{(1)}$ and $F_+^{(1)}$ curves of Fig. 3, increasing Q results in the output frequency becoming less dependent on the parameter G . For sufficiently large Q (e.g., $Q > 8$), the output frequency equals the ideal frequency 1 (normalized). The output signal v becomes closer to sinusoidal (with reduced harmonic content), but the Floquet exponent also increases, implying slower convergence towards to self-sustained oscillation, or locking in the case of

a frequency divider, as the rate of convergence is proportional to μ . Thus, for sufficiently large Q , the resistor R in the model (1) effectively appears in parallel with the L and C elements, a remark that will be utilized in analyzing the oscillator's operation under external excitation as a divider.

Finally, note that the presented analysis characterizes qualitatively a much larger class of LC oscillators with a single tank and differential active element, including, as a special case, the MOS architecture established in [1]. The extension of the bifurcation curves to the whole parameter space can be achieved numerically in a similar manner for any nonlinear function f and, thus, any such oscillator.

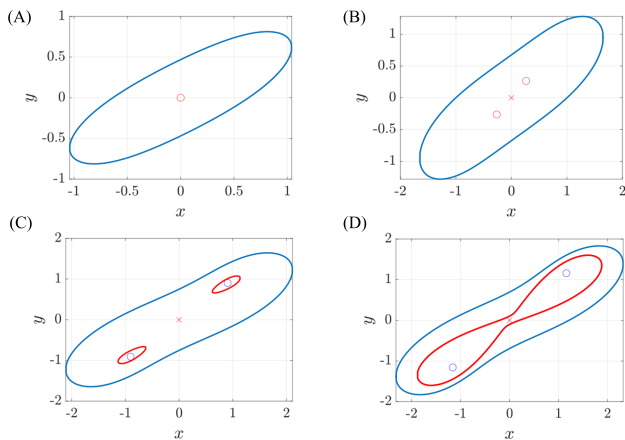


FIGURE 4. Phase portraits of system (3) describing the BJT implementation for parameters (G, Q) where (3) admits a stable limit cycle based on the bifurcation curves in Fig. 3. Blue: attractors, red: unstable entities, circles: nodes, crosses: saddles. Points (A), (B), (C), and (D) in the parameter space of Fig. 3 correspond to the respective phase plots.

III. Nonlinear Analysis of the Injection Locked Frequency Divider

In this section, the operation of the general signal-injected oscillator-model in Fig. 1, as a frequency divider, is analysed. The corresponding system-level diagram appears in Fig. 6. The external forcing affects directly the term $I_0(t)$ making it time-dependent and, in turn, causing $i_c = I_0(t)f(v/V_r)$ to be explicitly time-dependent as well. We express $I_0(t) = \Gamma g(\omega_{in}t; A)$, which can be considered as an one-parameter family of functions, where the normalized (with respect to V_r) amplitude of the forcing A is the parameter and $\omega_{in}t$ represents the argument. We adopt the above notation in order to stress that the two variables, A and $\omega_{in}t$, are treated as conceptually different. Function g can be considered as a (non-linear) transformation of the injected signal $AV_r \cos(\omega_{in}t)$. We assume that $g(\cdot; A)$ is 2π -periodic for every A and satisfies $g(\omega_{in}t; 0) = 1$ for all t -i.e., in the absence of any forcing, the current $I_0(t)$ equals its DC value. So, I_0 has angular frequency ω_{in} , normalized amplitude (with respect to V_r) A and Γ corresponds to the dc current value considered in Section II in the absence of external injection.

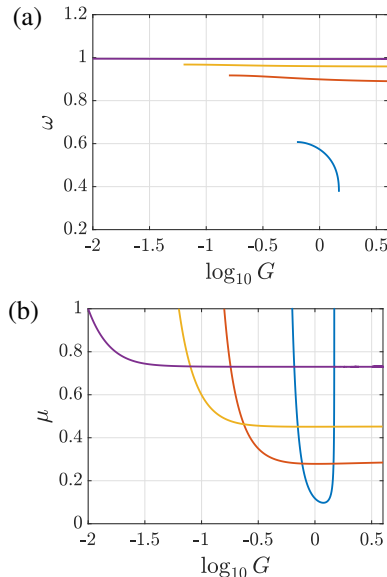


FIGURE 5. The effects of G and Q parameters on the Floquet multiplier and the (normalized) frequency of the limit cycle. Blue: $\log_{10} Q = 0.1$. Orange: $\log_{10} Q = 0.4$. Yellow: $\log_{10} Q = 0.6$. Magenta: $\log_{10} Q = 1$.

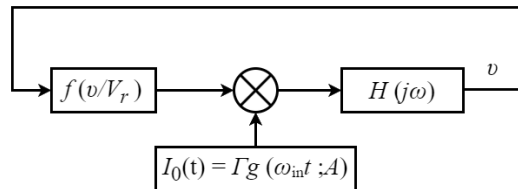


FIGURE 6. System diagram of the generic ILFD captured in Fig. 1.

We assume that Q is large enough, typically around 10, and that G satisfies $G < 1$, $Q^2G > 1$, i.e. the parameters lie between the $H^{(1)}$ and $F_+^{(1)}$ curves of Fig. 3. As shown in Section II, the free-running oscillator (1) has a natural frequency very close to $\omega_0 = 1/\sqrt{LC}$ and, as a result, we can approximate the equivalent model in Fig. 1, with the resistor R being in parallel with the L, C elements. The current to voltage natural frequency response of the filter is now expressed, with the assumption of large Q , nearby the resonance frequency ω_0 , as

$$H(j\omega) = \frac{H_0}{1 + j2Q\frac{\Delta\omega}{\omega_0}}, \quad \Delta\omega = \omega - \omega_0, \quad (10)$$

where H_0 is a constant with Ω dimensions. Assuming a general divide-by- N operation ($N > 1$), the abstract circuit in Fig. 1 has the system level model of Fig. 6, where $\omega_{in} = N\omega_{out}$. To establish the equivalence, we first note that the voltage-controlled current source $i_c(t)$, modeling the negative resistance, is the product of two distinct terms: the dimensionless nonlinear function $f(v/V_r)$ and the current $I_0(t) = \Gamma g(\omega_{in}t; A)$, where g is a function of the injected voltage. These two terms are represented independently in Fig. 6 in order to distinguish the nonlinearity f from the explicit time-dependence. Their product, i_c , is then the input of the filter R, L, C composed by the passive elements

H , whose output v , is the input of the nonlinear function f , resulting in the closed loop.

Since the value of Q is assumed large enough (and $G < 1$), the limit cycle is almost completely harmonic and the unique attractor. Thus, at steady state, the output voltage v is expressed as,

$$v = V_r B \cos(\omega_{\text{out}} t + \theta), \quad (11)$$

for some $B > 0$ and $\theta \in [0, 2\pi)$. Expanding the periodic signal $g(\omega_{\text{in}} t; A)$ in Fourier series we have,

$$g(\omega_{\text{in}} t; A) = a_0(A) + 2 \sum_{n=1}^{\infty} a_n(A) \cos(nN\omega_{\text{out}} t) + 2 \sum_{n=1}^{\infty} c_n(A) \sin(nN\omega_{\text{out}} t), \quad (12)$$

where

$$a_n(A) = \frac{1}{2\pi} \int_0^{2\pi} g(\phi; A) \cos(n\phi) d\phi \quad (13)$$

$$c_n(A) = \frac{1}{2\pi} \int_0^{2\pi} g(\phi; A) \sin(n\phi) d\phi.$$

Similarly, since $f(v/V_r)$ is even with respect to the argument $\phi = \omega_{\text{out}} t + \theta$, by expanding we get,

$$f(v/V_r) = b_0(B) + 2 \sum_{n=1}^{\infty} b_n(B) \cos(n\omega_{\text{out}} t + n\theta), \quad (14)$$

where

$$b_n(B) = \frac{1}{2\pi} \int_0^{2\pi} f(B \cos \phi) \cos(n\phi) d\phi. \quad (15)$$

The parity of f implies $b_{2n} = 0$ and thus the series in (14) contains only odd terms. Multiplying (15) with (12) we obtain,

$$g \cdot f = 2a_0(A) \sum_{m=1}^{\infty} b_{2m-1}(B) \cos[(2m-1)(\omega_{\text{out}} t + \theta)] + 2 \sum_{n=1}^{\infty} \sum_{m=1}^{\infty} a_n(A) b_{2m-1}(B) \left[\cos(\alpha_{n,m}(t)) + \cos(\beta_{n,m}(t)) \right] + 2 \sum_{n=1}^{\infty} \sum_{m=1}^{\infty} c_n(A) b_{2m-1}(B) \left[\sin(\alpha_{n,m}(t)) + \sin(\beta_{n,m}(t)) \right], \quad (16)$$

where we set

$$\alpha_{n,m}(t) = (nN - (2m-1))\omega_{\text{out}} t - (2m-1)\theta, \quad (17)$$

and

$$\beta_{n,m}(t) = (nN + (2m-1))\omega_{\text{out}} t + (2m-1)\theta. \quad (18)$$

Our assumption for large Q implies that the bandpass filter H rejects all intermodulation products away from ω_0 . Considering that ω_{out} lies sufficiently close to ω_0 , the indices m and n of the terms in the double summation in (16) that pass through the filter must satisfy $nN - (2m-1) = \pm 1 \Rightarrow m = (nN + 1 \mp 1)/2$. The cases $nN + (2m-1) = \pm 1$ lead to no solution, since the corresponding frequencies are rejected by H . Let S denote the set of integers to which n

belongs, so that m is also an integer. If N is even, then n is unconstrained and traverses all positive integers. If N is odd, then S contains only the even positive integers.

Based on the preceding discussion, the terms in (16) that pass through the filter are given by

$$2a_0(A)b_1(B) \cos(\omega_{\text{out}} t + \theta) + 2 \sum_{n \in S} \left[a_n(A)b_{nN-1}(B) \cos(\omega_{\text{out}} t - (nN-1)\theta) + a_n(A)b_{nN+1}(B) \cos(\omega_{\text{out}} t + (nN+1)\theta) \right] + 2 \sum_{n \in S} \left[c_n(A)b_{nN-1}(B) \sin(\omega_{\text{out}} t - (nN-1)\theta) - c_n(A)b_{nN+1}(B) \sin(\omega_{\text{out}} t + (nN+1)\theta) \right]. \quad (19)$$

Writing (19) in phasor form and applying the filter H , we derive the following complex equation

$$V_r B e^{j\theta} = \frac{2H_0\Gamma}{1 + 2jQ \frac{\Delta\omega}{\omega_0}} \left\{ a_0(A)b_1(B)e^{j\theta} + \sum_{n \in S} \left[a_n(A) \left(b_{nN-1}(B)e^{-j(nN-1)\theta} + b_{nN+1}(B)e^{j(nN+1)\theta} \right) - jc_n(A) \left(b_{nN-1}(B)e^{-j(nN-1)\theta} - b_{nN+1}(B)e^{j(nN+1)\theta} \right) \right] \right\} \quad (20)$$

where $\Delta\omega$ is evaluated at ω_{out} , namely $\Delta\omega = \omega_{\text{out}} - \omega_0$. Separating the real and imaginary parts and dividing them, we get

$$\Delta\omega(\theta) = \frac{\omega_0}{2Q} \frac{P(\theta)}{D(\theta)}. \quad (21)$$

The functions $P(\theta)$ and $D(\theta)$ are given by the relations

$$P(\theta) = \sum_{n \in S} d_n(B) \left(a_n(A) \sin(nN\theta) + c_n(A) \cos(nN\theta) \right) \quad (22)$$

$$D(\theta) = b_1(B)a_0(A) + \sum_{n \in S} s_n(B) \left(a_n(A) \cos(nN\theta) - c_n(A) \sin(nN\theta) \right), \quad (23)$$

where the coefficients s_n, d_n are expressed as,

$$s_n(B) = b_{nN+1}(B) + b_{nN-1}(B) \quad (24)$$

$$d_n(B) = b_{nN+1}(B) - b_{nN-1}(B).$$

The maximum two-sided output referred locking range for the divide-by- N operation is given by,

$$\widehat{\Delta\omega}_{\text{max}} = \frac{\omega_0}{Q} \max_{\theta \in [0, 2\pi)} \frac{P(\theta)}{D(\theta)}. \quad (25)$$

We remark that the condition $\Delta\omega \leq \widehat{\Delta\omega}_{\text{max}}$ is necessary and sufficient for (20) to admit a solution. Riemann-Lebesgue Lemma [49] ensures that $\lim_{n \rightarrow \infty} a_n, b_n, c_n = 0$ so that terms in (22) of high index can be ignored in practical

TABLE 1. Output-referred Locking Range estimation for even N and even

$I_0(t) = \Gamma g(\omega_{in}t; A)$.

Number of Terms	Locking Range Estimation $\times Q/\omega_0$
1 Term	$\frac{ a_1 d_1 }{\sqrt{a_0^2 b_1^2 - a_1^2 s_1^2}}$
2 Terms	$\max_{\theta \in [0, 2\pi]} \frac{a_1 d_1 \sin(N\theta) + a_2 d_2 \sin(2N\theta)}{b_1 a_0 + a_1 s_1 \cos(N\theta) + a_2 s_2 \cos(2N\theta)}$
k Terms	$\max_{\theta \in [0, 2\pi]} \frac{a_1 d_1 \sin(N\theta) + \dots + a_k d_k \sin(kN\theta)}{b_1 a_0 + a_1 s_1 \cos(N\theta) + \dots + a_k s_k \cos(kN\theta)}$

calculations and a truncated Fourier series be utilized. Further, if for a given N , the terms decrease fast enough, one can consider only the first term in (22) and approximate $\Delta\omega$ by

$$\Delta\omega = \frac{\omega_0}{2Q} \frac{C_1 \sin(nN\theta) + C_2 \cos(nN\theta)}{C_3 + C_4 \cos(nN\theta) + C_5 \sin(nN\theta)}, \quad (26)$$

where $n = 1$ or $n = 2$,

$$C_1 = a_n(A)d_n(B), \quad C_2 = c_n(A)d_n(B), \quad (27)$$

and

$$C_3 = a_0(A)b_1(B), \quad C_4 = a_n(A)s_n(B), \quad C_5 = -c_n(A)s_n(B). \quad (28)$$

In particular if $I_0(t)$ is even, then $c_n = 0$ and assuming $|C_4/C_3| < 1$, (26) has a maximum for $\cos(nN\theta) = -C_4/C_3$ which results in the approximate two-sided output referred locking range

$$\widehat{\Delta\omega}_{\max} = \frac{\omega_0}{Q} \frac{|C_1|}{\sqrt{C_3^2 - C_4^2}}. \quad (29)$$

We note that based on the equations (22) and (23), the approximation of (29) with even I_0 is equivalent to approximating the injected signal g as having only one harmonic. However, it still provides a better approximation than Adler's equation, since the full nonlinear function f is considered in the derivation instead of its linear approximation. If more terms are considered in the series (22) then the maximum can be found numerically in a straightforward manner. We note that in practical calculations, under the assumption of weak injection, the amplitude B in the previous relations, can be approximated by the (normalized) free-running amplitude. Table 1 summarizes the approximation using the first k terms in (22) for the maximum locking range in the case of even N , where we have dropped the explicit dependence of a , b , s , and d on A and B . Modifications for the cases of odd N and arbitrary I_0 are straightforward.

As discussed in Section II, the parameters (G, Q) influence the characteristics of the limit cycle and, consequently, the maximum locking range. Although this topic lies beyond the

scope of the present work, an interesting direction for future research would be to investigate this dependence, based on the proposed analysis, for optimization purposes.

Application to the Complementary BJT ILFD

In particular, if one considers the circuit of Fig. 2, then (8) implies that $b_n(B)$ corresponds to the n -th Fourier coefficient in the expansion of $\tanh(B \cos(\theta))$ and $a_n(A)$, $c_n(A)$ to the n -th Fourier coefficients of $g(\omega_{in}t; A) = \exp(AV_r \cos(\omega_{in}t))$. Thus, $a_n(A) = I_n(A)$, $c_n(A) = 0$ where $I_n(\cdot)$ denotes the n -th modified Bessel function of the first kind. In the case $N = 2$, (29) is in agreement with the result in [46].

Fig. 8 compares the theoretical results, considering different numbers of terms in the summations in (25) (c.f. Table 1), with the experimentally measured input-referred LR using the implementation shown in Fig. 7. We note that the input-referred LR is twice that of the output-referred LR. For this reason, the formulae in (29) and Table 1 are multiplied by two. Adler's line, which has been included for comparison, has a slope equal to the parameter G for a differential LC oscillator. The parameters of the ILFD in Fig. 2, as implemented in Fig. 7, were selected such that the free-running frequency equals $f_0 = 128$ MHz, $Q = 10$, $G < 1$ and $Q^2 G > 1$, which, as theoretically expected, results in an almost harmonic free-running oscillator. More specifically, the values of the passive elements are $L = 25$ nH, $C = 62$ pF and the parasitic resistor R was measured around 2Ω . The bias current equals 2 mA, resulting in $G = 0.08$. The NPN transistor model is HFA3134, while the PNP transistor model is HFA3135, characterized by $\beta = 200$ and $\beta = 125$, respectively¹. The measurement of the experimental locking range was performed using a brute-force approach. Specifically, the Lissajous figure on the oscilloscope, between the injected voltage signal and the voltage across the capacitor, was used to determine whether locking occurred—equivalently, whether the curve was closed or not. For different values of the injected amplitude, A , the injected frequency f_{in} was gradually increased (decreased) from $2f_0 = 256$ MHz until synchronization was destroyed, resulting in the maximum (minimum) input frequency that achieves 2 : 1 locking, i.e., an output frequency equal to half of the input frequency. The difference between these frequencies equals the experimental input-referred locking range (LR), shown in Fig. 8.

Considering only one term (equivalent to (29)), for small injection voltages, the locking range is accurately estimated by the analytical expression (29). This first-order approximation, however, deviates from the measurements as the injection voltage increases, providing a conservative estimation. Considering two terms, the theoretical curve approximates both the qualitative and quantitative aspects of the experimental results. Further, this validates the strong decreasing nature of the higher-order terms in the summations (22), (22), as explained in Section III. Thus, at the first stage of the design

¹More information about their characteristics can be found at the following link to the datasheet [link].

(29) can be used to provide a worst-case estimation and, if better accuracy is needed at larger injection voltages, more terms (only two) from Table 1 can be used.

If we considered a different architecture of a differential LC divider, then we would follow the same procedure. It can be described as follows:

- Determine the nonlinearity f and consider an inductor such that Q is at least 10 (as demonstrated, the qualitative behavior is similar). Ensure that $Q^2G > 1$ and $G < 1$.
- Determine I_0 , or equivalently g , and the set S , based on N .
- Compute the coefficients a_n, c_n from (13), b_n from (15) and thus s_n, d_n from (24).
- To obtain a first-order estimate consider only the first term in (22) and (23). Maximize (26) where the C_i coefficients are given by (27) and (28). If I_0 is even, (29) holds.
- If better accuracy is needed, consider more terms in the summation of P, D in (22), (23), and numerically maximize (25). If N and I_0 are even, Table 1 applies.

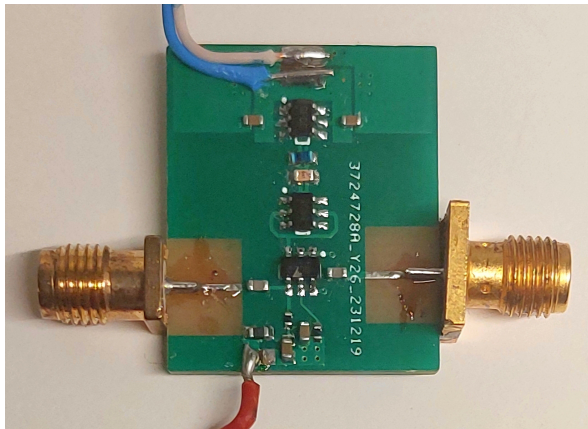


FIGURE 7. Experimental implementation of the circuit shown in Fig. 2 for measuring the LR.

IV. Conclusions

Considering a general class of differential LC oscillators, we first conducted a bifurcation analysis regarding the design parameters and discussed the conditions necessary for a stable limit cycle to exist. We demonstrated that all oscillators within this class exhibit the same qualitative behavior, at least in a neighborhood of the origin. By using the complementary BJT oscillator as an example, we showed how the bifurcation curves of such an oscillator are numerically extended, deducing, thus, quantitative oscillatory conditions and validating the qualitative general results. Subsequently, we investigated the harmonically forced oscillator as a frequency divider. We introduced a comprehensive nonlinear approach based on the Harmonic Balance technique to estimate analytically the locking range under weak injection conditions. The

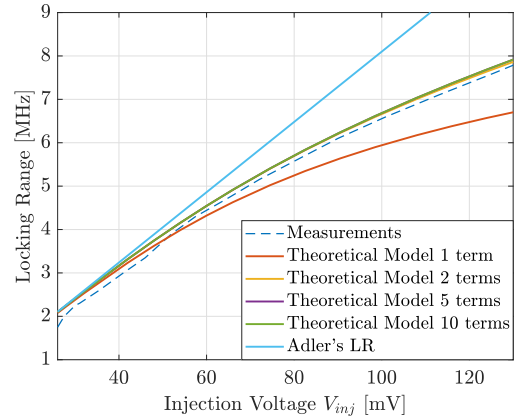


FIGURE 8. Theoretical and measured two sided input-referred locking-range considering the circuit in Fig. (2) and divide by 2 operation. Free running frequency $f_0 = 128$ MHz and $Q = 10$.

final formulae are easily evaluated and can be viewed as a generalization of Adler's equations. The application of this methodology to the complementary BJT oscillator yielded results closely aligned with the measurements, complementing the approach presented in [46].

REFERENCES

- [1] S. Daneshgar, O. De Feo, and M. P. Kennedy, "Observations concerning the locking range in a complementary differential LC injection-locked frequency divider—Part I: Qualitative analysis," *IEEE Transactions on Circuits and Systems I: Regular Papers*, vol. 57, no. 1, pp. 179–188, 2010.
- [2] B. Hong and A. Hajimiri, "A general theory of injection locking and pulling in electrical oscillators—Part I: Time-synchronous modeling and injection waveform design," *IEEE Journal of Solid-State Circuits*, vol. 54, no. 8, pp. 2109–2121, 2019.
- [3] A. Hajimiri and T. Lee, "Design issues in CMOS differential LC oscillators," *IEEE Journal of Solid-State Circuits*, vol. 34, no. 5, pp. 717–724, 1999.
- [4] J. Guckenheimer and P. Holmes, *Nonlinear Oscillations, Dynamical Systems, and Bifurcations of Vector Fields*. Springer-Verlag, 1983.
- [5] S. Wiggins, *Introduction to Applied Nonlinear Dynamical Systems and Chaos*, 2nd ed. Springer-Verlag, 2003.
- [6] Y. A. Kuznetsov, *Elements of Applied Bifurcation Theory*, 3rd ed. Springer-Verlag, 2004.
- [7] Y. A. Kuznetsov, S. Muratori, and S. Rinaldi, "Bifurcations and chaos in a periodic predator-prey model," *International Journal of Bifurcation and Chaos*, vol. 02, no. 01, pp. 117–128, 1992.
- [8] T. Bakri, Y. A. Kuznetsov, and F. Verhulst, "Torus bifurcations in a mechanical system," *Journal of Dynamics and Differential Equations*, vol. 27, pp. 371–403, 2015.
- [9] Y. Zhiyenbayev, Y. Kominis, C. Valagiannopoulos, V. Kovanis, and A. Bountis, "Enhanced stability, bistability, and exceptional points in saturable active photonic couplers," *Phys. Rev. A*, vol. 100, p. 043834, Oct 2019.
- [10] S. Christou, V. Kovanis, A. E. Giannakopoulos, and Y. Kominis, "Parametric control of self-sustained and self-modulated optomechanical oscillations," *Phys. Rev. A*, vol. 103, p. 053513, May 2021.
- [11] G. Maggio, O. De Feo, and M. Kennedy, "Nonlinear analysis of the Colpitts oscillator and applications to design," *IEEE Transactions on Circuits and Systems I: Fundamental Theory and Applications*, vol. 46, no. 9, pp. 1118–1130, 1999.
- [12] O. De Feo, G. Maggio, and M. Kennedy, "The Colpitts oscillator: Families of periodic solutions and their bifurcations," *International Journal of Bifurcation and Chaos*, vol. 10, 05 2012.
- [13] H. de Blank, Y. Kuznetsov, M. Pekkér, and D. Veldman, "Degenerate Bogdanov–Takens bifurcations in a one-dimensional transport model

- of a fusion plasma," *Physica D: Nonlinear Phenomena*, vol. 331, pp. 13–26, 2016.
- [14] S. P. Hastings, "On the existence of homoclinic and periodic orbits for the FitzHugh-Nagumo equations," *The Quarterly Journal of Mathematics*, vol. 27, no. 1, pp. 123–134, 03 1976.
- [15] A. Pikovsky, M. Rosenblum, and J. Kurths, *Synchronization: A Universal Concept in Nonlinear Sciences*, ser. Cambridge Nonlinear Science Series. Cambridge University Press, 2001.
- [16] P. Maffezzoni, "Synchronization analysis of two weakly coupled oscillators through a PPV macromodel," *IEEE Transactions on Circuits and Systems I: Regular Papers*, vol. 57, no. 3, pp. 654–663, 2010.
- [17] R. Adler, "A study of locking phenomena in oscillators," *Proceedings of the IRE*, vol. 34, no. 6, pp. 351–357, 1946.
- [18] A. Buonomo and A. Lo Schiavo, "A study of injection locking in dual-band CMOS frequency dividers," *IEEE Transactions on Circuits and Systems I: Regular Papers*, vol. 64, no. 5, pp. 1225–1234, 2017.
- [19] —, "Nonlinear dynamics of divide-by-two injection-locked frequency dividers in locked operation mode," *International Journal of Circuit Theory and Applications*, vol. 42, no. 8, pp. 794–807, 2014. [Online]. Available: <https://onlinelibrary.wiley.com/doi/abs/10.1002/cta.1888>
- [20] —, "Locking range of frequency dividers with dual-resonance tank," *IEEE Transactions on Circuits and Systems II: Express Briefs*, vol. 65, no. 5, pp. 597–601, 2018.
- [21] —, "Analytical approach to the study of injection-locked frequency dividers," *IEEE Transactions on Circuits and Systems I: Regular Papers*, vol. 60, no. 1, pp. 51–62, 2013.
- [22] —, "A deep investigation of the synchronization mechanisms in LC-CMOS frequency dividers," *IEEE Transactions on Circuits and Systems I: Regular Papers*, vol. 60, no. 11, pp. 2857–2866, 2013.
- [23] A. Buonomo, M. P. Kennedy, and A. L. Schiavo, "On the synchronization condition for superharmonic coupled QVCOs," *IEEE Transactions on Circuits and Systems I: Regular Papers*, vol. 58, no. 7, pp. 1637–1646, 2011.
- [24] A. Buonomo and A. L. Schiavo, "Modelling and analysis of differential VCOs," *International Journal of Circuit Theory and Applications*, vol. 32, no. 3, pp. 117–131, 2004.
- [25] A. Buonomo and A. Lo Schiavo, "Mode dynamics in fourth-order LC oscillators," *International Journal of Circuit Theory and Applications*, vol. 45, no. 8, pp. 1049–1059, 2017.
- [26] A. Buonomo, A. L. Schiavo, M. A. Awan, M. S. Asghar, and M. P. Kennedy, "A CMOS injection-locked frequency divider optimized for divide-by-two and divide-by-three operation," *IEEE Transactions on Circuits and Systems I: Regular Papers*, vol. 60, no. 12, pp. 3126–3135, 2013.
- [27] A. Buonomo and A. L. Schiavo, "Investigation of modes in double-tuned LC-VCOs," *IEEE Transactions on Circuits and Systems I: Regular Papers*, vol. 63, no. 6, pp. 905–915, 2016.
- [28] P. Maffezzoni, "Analysis of oscillator injection locking through phase-domain impulse-response," *IEEE Transactions on Circuits and Systems I: Regular Papers*, vol. 55, no. 5, pp. 1297–1305, 2008.
- [29] —, "Analysis of oscillator injection locking through phase-domain impulse-response," *IEEE Transactions on Circuits and Systems I: Regular Papers*, vol. 55, no. 5, pp. 1297–1305, 2008.
- [30] P. Maffezzoni, D. D'Amore, S. Daneshgar, and M. P. Kennedy, "Analysis and design of injection-locked frequency dividers by means of a phase-domain macromodel," *IEEE Transactions on Circuits and Systems I: Regular Papers*, vol. 57, no. 11, pp. 2956–2966, 2010.
- [31] B. Hong and A. Hajimiri, "A general theory of injection locking and pulling in electrical oscillators—Part II: Amplitude modulation in LC oscillators, transient behavior, and frequency division," *IEEE Journal of Solid-State Circuits*, vol. 54, no. 8, pp. 2122–2139, 2019.
- [32] A. Buonomo, "Nonlinear analysis of voltage-controlled oscillators: A systematic approach," *IEEE Transactions on Circuits and Systems I: Regular Papers*, vol. 55, no. 6, pp. 1659–1670, 2008.
- [33] S. Verma, H. Rategh, and T. Lee, "A unified model for injection-locked frequency dividers," *IEEE Journal of Solid-State Circuits*, vol. 38, no. 6, pp. 1015–1027, 2003.
- [34] R. Quere, E. Ngoya, M. Camiade, A. Suarez, M. Hessane, and J. Obregon, "Large signal design of broadband monolithic microwave frequency dividers and phase-locked oscillators," *IEEE Transactions on Microwave Theory and Techniques*, vol. 41, no. 11, pp. 1928–1938, 1993.
- [35] L. Pantoli, A. Suarez, G. Leuzzi, and F. Di Paolo, "Complete and systematic simulation tools for frequency divider design," *IEEE Transactions on Microwave Theory and Techniques*, vol. 56, no. 11, pp. 2442–2452, 2008.
- [36] A. Collado, F. Ramirez, A. Suarez, and J. Pascual, "Harmonic-Balance analysis and synthesis of coupled-oscillator arrays," *IEEE Microwave and Wireless Components Letters*, vol. 14, no. 5, pp. 192–194, 2004.
- [37] F. Ramirez, S. Sancho, and A. Suárez, "Oscillation modes in multiresonant oscillator circuits," *IEEE Transactions on Microwave Theory and Techniques*, vol. 64, no. 12, pp. 4660–4675, 2016.
- [38] A. Suarez, "Check the stability: Stability analysis methods for microwave circuits," *IEEE Microwave Magazine*, vol. 16, no. 5, pp. 69–90, 2015.
- [39] A. Suarez, S. Sancho, and F. Ramirez, "General formulation for the analysis of injection-locked coupled-oscillator systems," *IEEE Transactions on Microwave Theory and Techniques*, vol. 61, no. 12, pp. 4730–4744, 2013.
- [40] A. Suárez and F. Ramírez, "Two-level stability analysis of complex circuits," *IEEE Transactions on Microwave Theory and Techniques*, vol. 69, no. 1, pp. 132–146, 2021.
- [41] R. Quere, E. Ngoya, M. Camiade, A. Suarez, M. Hessane, and J. Obregon, "Large signal design of broadband monolithic microwave frequency dividers and phase-locked oscillators," *IEEE Transactions on Microwave Theory and Techniques*, vol. 41, no. 11, pp. 1928–1938, 1993.
- [42] A. Collado, F. Ramirez, A. Suarez, and J. Pascual, "Harmonic-balance analysis and synthesis of coupled-oscillator arrays," *IEEE Microwave and Wireless Components Letters*, vol. 14, no. 5, pp. 192–194, 2004.
- [43] F. Ramirez, M. Ponton, S. Sancho, and A. Suarez, "Phase-noise analysis of injection-locked oscillators and analog frequency dividers," *IEEE Transactions on Microwave Theory and Techniques*, vol. 56, no. 2, pp. 393–407, 2008.
- [44] U. Yodprasit and C. Enz, "Nonlinear analysis of a Colpitts injection-locked frequency divider," in *Proceedings of the 2003 International Symposium on Circuits and Systems, 2003. ISCAS '03.*, vol. 1, 2003, pp. I–I.
- [45] B. Hong and A. Hajimiri, "A phasor-based analysis of sinusoidal injection locking in LC and ring oscillators," *IEEE Transactions on Circuits and Systems I: Regular Papers*, vol. 66, no. 1, pp. 355–368, 2019.
- [46] K. Metaxas, V. Alimisis, N. P. Eleftheriou, and P. P. Sotiriadis, "Non-linear analysis and simulation of an injection locked frequency divider using a complementary BJT oscillator," in *2024 Panhellenic Conference on Electronics and Telecommunications (PACET)*, 2024, pp. 1–4.
- [47] J. Carr, *Applications of Centre Manifold Theory*. Springer-Verlag, 1983.
- [48] A. Dhooge, W. Govaerts, and Y. A. Kuznetsov, "MATCONT: A MATLAB package for numerical bifurcation analysis of odes," *ACM Trans. Math. Softw.*, vol. 29, no. 2, p. 141–164, jun 2003. [Online]. Available: <https://doi.org/10.1145/779359.779362>
- [49] L. Grafakos, *Classical Fourier Analysis*. Springer-Verlag, 2014.



Konstantinos Metaxas received the M.Eng. degree (summa cum laude) in Electrical and Computer Engineering from the National Technical University of Athens in 2024. He has received several academic awards during his studies. His research interests include nonlinear dynamics, control theory, applied mathematics and nonlinear electronic circuits.



Vassilis Alimisis (Member, IEEE) is an Analog IC Design Engineer and AI Computing Researcher. He received the B.Sc. in Physics (top 1%) and the M.Sc. degree in Electronics and Communications from the University of Patras, Greece, in July 2017 and March 2019 respectively. He received the Ph.D. degree from the National Technical University of Athens (NTUA), Greece, under the supervision of Professor Paul P. Sotiriadis in June 2024. His Ph.D. Thesis entitled "Integrated circuit architectures for classical and neural computing with applications

in artificial intelligence" and research were supported and financed by the E.L.K.E. NTUA Scholarships. Currently, he is an Adjunct Lecturer at the Department of Digital Industry Technologies, National and Kapodistrian University of Athens (NKUA), a Senior Researcher at Archimedes/Athena Research Center and Postdoctoral Researcher at the School of Electrical and Computer Engineering, NTUA, Athens, Greece. During his PhD, he was a Teaching Assistant in undergraduate and graduate courses and supervised several Diploma Theses (more than 20). He has authored and co-authored several journal articles and conference papers (more than 60 publications). His main research interests include analog microelectronic circuits, low power electronics, analog computing and integrated circuit architectures with applications in artificial intelligence and machine learning. He has received the Best Paper Award in the IEEE Int. Conf. on Microelectronics 2020, the Best Paper Award in the IEEE Int. Conf. on Microelectronics 2021, the Best Paper Award (3rd Place) in the IEEE Int. Conf. on Microelectronics 2023, the Best Paper Award in IEEE Symposium on Integrated Circuits and Systems Design (SBCCI) 2021, the Best Runner-Up PhD Symposium Paper Award in the 1st International Conference on Frontiers of Artificial Intelligence, Ethics, and Multidisciplinary Applications in 2023 and the Best PhD Symposium Paper Award in the 2nd International Conference on Frontiers of Artificial Intelligence, Ethics, and Multidisciplinary Applications in 2024. He regularly reviews for many IEEE transactions and conferences and serves on proposal review panels.



Costas Oustoglou received the Diploma degree in Electrical and Computer Engineering from the National Technical University of Athens, Athens, Greece, in 2017. He is currently pursuing the Ph.D. degree with the National Technical University of Athens, under the supervision of Prof. Paul P. Sotiriadis. His main research interests include radiometry systems and applications, and design and development of embedded and mixed signal systems. Mr. Oustoglou is a regular reviewer for many IEEE publications.



Yanniss Kominis is an Associate Professor in the School of Applied Mathematical and Physical Sciences of the National Technical University of Athens (NTUA). He holds a Diploma (1997) and a PhD (2003) from the School of Electrical and Computer Engineering of NTUA. His research interests include the study of complex dynamics of nonlinear systems and the nonlinear wave propagation in complex media, with applications to semiconductor lasers and photonics as well as in fusion plasmas. His work has been published

in more than 90 refereed papers and presented more than 80 times in international conferences and workshops. He serves as a reviewer in several high-impact journals and has supervised several Master's and PhD students as well as postdoctoral researchers. He is also a National Representative for Fusion in the EURATOM Programme Committee, a member of the Fusion Expert Group of the European Commission, and a member of the Steering Committee of the Hellenic National Fusion Research Programme.



Paul P. Sotiriadis (Fellow, IEEE) is a Professor of Electrical and Computer Engineering (ECE) at the National Technical University of Athens (NTUA), Greece. He is the Director of the Electronics Laboratory at NTUA and a governing board member of the Hellenic (National) Space Center of Greece.

His research interests include the design, optimization, and mathematical modeling of Analog, mixed-signal and RF integrated and discrete circuits, sensor and instrumentation architectures with emphasis in biomedical instrumentation, advanced RF frequency synthesis, and, the application of Machine Learning and general AI in the operation as well as the design of electronic circuits. He runs a team of 20 researchers.

He received the Diploma degree in ECE from NTUA in 1994 with the highest ever GPA, the MS degree in Electrical Engineering from Stanford University, and the Ph.D. degree in Electrical Engineering and Computer Science from the M.I.T. in 2002. Immediately after completing his Ph.D., he joined the faculty of the Johns Hopkins University ECE department, and in 2012 he joined the faculty of the ECE department at NTUA. He has authored and co-authored more than 220 research publications, most of them in IEEE journals and conferences and has contributed several chapters to technical books.

He has received numerous awards, including the prestigious 2012 IEEE Guillemin-Cauer Award, Best Paper Awards at IEEE ICM 2023, FIAEMA 2023, IEEE ICM 2021, IEEE SBCCI 2021, IEEE ICM 2020, IEEE MOCAS 2019, IEEE IFCS 2012, IEEE ISCAS 2007, and SBCCI 2007, the Broadcom Foundation USA Research Award, and the 2022 IEEE CAS Outstanding Technical Committee Recognition. He has been listed among Stanford's top 2% most influential researchers in the world in 2019, 2020, 2021, 2022 and 2023.

He is an Associate Editor of the IEEE Open Journal of Circuits and Systems and the IEEE Sensors Journal, has served as an Associate Editor of the IEEE Transactions on Circuits and Systems – I (2016-2020) and the IEEE Transactions on Circuits and Systems – II (2005-2010), was a member of the IEEE CAS Fellows Evaluation Committee (FEC), and has been a member of technical committees of many conferences. He regularly reviews for many IEEE transactions and conferences and serves on proposal review panels.